Respiratory Research

RESEARCH

Open Access

Inhaled tea polyphenol-loaded nanoparticles coated with platelet membranes largely attenuate asthmatic inflammation

Suidong Ouyang[1*†], Peishan Lu[1†], Jianing Li[1], Hua Jin[3], Wanhua Wu[1], Renxing Luo[1], Bin Wang[1], Xueqin Huang[1], Xinlong Lian[2] and Gonghua Huang[1*]

Abstract

Background Tea polyphenols (TPs), prominent constituents of green tea, possess remarkable antioxidant and anti-inflammatory properties. However, their therapeutic potential is limited due to low absorption and poor bioavailability. To address this limitation and enhance their efficacy, we developed a biomimetic nanoplatform by coating platelet membrane (PM) onto poly-lactic-co-glycolic acid (PLGA) nanoparticles (NPs) to create targeted delivery vehicles for TPs (PM@TP/NPs) to the inflamed tissues in asthma.

Methods After synthesizing and characterizing PM@TP/NPs, we assessed their biocompatibility and biosafety through cell viability assays, hemolysis tests, and inflammation analysis in vivo and in vitro. The therapeutic effect of PM@TP/NPs on asthma was then evaluated using a mouse model of HDM-induced asthma. Additionally, PM@TP/NPs-mediated reactive oxygen species (ROS) scavenging capacity, as well as the activation of signaling pathways, were analyzed in HBE cells and asthmatic mice via flow cytometry, RT-qPCR, and western blotting.

Results Compared with free TPs, PM@TP/NPs demonstrated excellent biocompatibility and safety profiles in both in vitro and in vivo, as well as enhanced retention in inflamed lungs. In HDM-induced mouse asthma model, inhaled PM@TP/NPs largely attenuated lung inflammation and reduced the secretion of type 2 pro-inflammatory cytokines in the lungs compared to free TPs. The therapeutic effects of PM@TP/NPs on asthma might be associated with an enhanced ROS scavenging capacity, increased activation of the Nrf2/HO-1 pathway, and decreased activation of the CCL2/MAPK and TLR4/NF-κB pathway in the lungs.

Conclusions Our findings demonstrate that inhalation of PM@TP/NPs largely attenuated lung inflammation in HDM-induced asthmatic mice. These results suggest that PM@TP/NPs might be a novel therapeutic strategy for asthma.

Keywords Tea polyphenols, Biomimetic nanoparticles, Platelet membrane, Asthma

†Suidong Ouyang and Peishan Lu contributed equally to this work.

*Correspondence:
Suidong Ouyang
ouyangsd@gdmu.edu.cn
Gonghua Huang
gonghua.huang@gdmu.edu.cn

[1]Guangdong Provincial Key Laboratory of Medical Molecular Diagnostics, The First Dongguan Affiliated Hospital, College of Medical Technology, Guangdong Medical University, Dongguan 523808, China
[2]Liaobu Hospital of Dongguan City, Dongguan 523430, China
[3]College of Pharmacy, Guangdong Medical University, Dongguan 523808, China

Introduction

Tea polyphenols (TPs), prominent constituents of green tea, exhibit diverse biological effects including antioxidant, anti-inflammatory, anti-tumor, and immunomodulatory activities, making them valuable for biomedical applications across various conditions such as autoimmune and neurodegenerative diseases [1, 2]. Recently, numerous studies have reported that the protective effects of Epigallocatechin-3-gallate (EGCG), which is the major polyphenol extracted from green tea, against asthma and other lung diseases [3–5]. For instance, EGCG inhibits airway inflammation and epithelial- mesenchymal transition through the PI3K/AKT pathway via upregulation of PTEN in ovalbumin (OVA)-challenged asthmatic mice [6]. However, its therapeutic efficacy is hindered by low absorption, poor bioavailability, and off-target effects [7].

In recent years, membrane-coated nanomedicines have been widely used for the targeted therapy of different diseases like inflammatory diseases, infection diseases, cardiovascular disease, and cancer [8]. Platelet membrane-coated NPs has recently attracted increasing attention due to the protein profile on platelet surfaces, which allows natural pathophysiological affinity and targeting to sites of inflammation, pathogens, vascular distress, and tumors [9, 10]. Previous studies have shown that the platelet camouflage technique is effective in treating certain pulmonary inflammatory diseases such as pneumonia and asthma, owing to their outstanding biocompatibility, long blood circulation, low immunogenicity, and selective targeting ability [11, 12]. Our previous studies utilizing platelet membrane-coated Berberine biomimetic nanoparticles demonstrated improved biocompatibility, bioavailability, and lung targeting, effectively attenuating allergic asthma [13]. However, the use of Tea polyphenols nanoparticles for asthma treatment as antioxidants and anti-inflammatory agents remains unexplored.

In asthma, various pro-inflammatory cytokines including TNF, IL-1β, IL-6, and reactive oxygen species (ROS) such as hydroxyl radicals and peroxides are overexpressed [14], contributing to oxidative stress and inflammation, which may culminate in airway tissue damage [15]. The pivotal role of ROS in asthma pathogenesis has been extensively studied, with oxidative stress linked to airway bronchoconstriction and hyperresponsiveness [16–18]. Consequently, inhibiting oxidative activity emerges as a potential strategy to mitigate asthma pathogenesis.

In this study, we synthesized platelet membrane-coated tea polyphenols biomimetic nanoparticles (PM@TP/NPs) and evaluated their therapeutic efficacy in a model of HDM-induced asthma. Our findings demonstrate that PM@TP/NPs efficiently alleviate oxidative stress and inflammation in vitro, leading to reduced ROS and inflammatory cytokine production. Furthermore, in an HDM-induced asthma mouse model, inhaled PM@TP/NPs effectively mitigate lung inflammation by scavenging ROS production while concurrently activing Nrf2/HO-1 signaling pathway and suppressing the CCL2/MAPK and TLR4/NF-κB signaling pathway. Collectively, our results suggest that PM@TP/NPs may offer a synergistic therapeutic approach for preventing and attenuating asthma.

Materials and methods

Mice

Female C57BL/6 mice aged 6–8 weeks were procured from Guangdong Experimental Animal Center (Guangzhou, China). They were housed in the animal facility of Guangdong Medical University under controlled conditions at 25.0±2 °C with a 12 h/12 h light-dark cycle. All animal procedures strictly adhered to the Guidelines for the Care and Use of Laboratory Animals of Guangdong Medical University. The Institutional Animal Care and Use Committee of Guangdong Medical University reviewed and approved all experimental protocols (GDY2002326).

Preparation of TP-loaded nanoparticles (TP/NPs)

The TP/NPs were synthesized using emulsification and evaporation methods as previously described with minor adjustments [19]. In brief, 20 mg of TP (Sigma-Aldrich, USA) and 160 mg of PLGA-PEG (lactide: glycolide 50:50, Sigma-Aldrich, USA) were co-dissolved in 5 mL of dichloromethane, serving as the oil phase (O). Meanwhile, 20 mL of PVA solution (1%, w/w, Sigma-Aldrich, USA) was prepared as the water phase (W). The oil phase was initially emulsified using ultrasonication for 40 s at 100 Watts on ice. Subsequently, the emulsified oil phase was added dropwise into the water phase, followed by a second emulsification through ultrasonication for an additional 40 s. To incorporate the nanoparticle fluorescence marker, 250 μg of Coumarin 6 (Cou6, Sigma, USA) was introduced into the oil phase. Finally, the nanoparticles were collected via centrifugation at 12,000 rpm for 20 min, followed by three washes with ultrapure water.

Synthesis of platelet membrane (PM)-coated TP-loaded NPs (PM@ TP/NPs)

Fresh whole blood was obtained from 8-week-old normal mice via cardiac puncture after euthanasia using CO_2. Platelets were then isolated from mouse blood using gradient centrifugation following established protocols [13]. Initially, the supernatant of 0.5 mL of mouse whole blood was centrifuged at 200 g for 10 min to yield platelet-rich plasma (PRP). Subsequently, PRP was separated from the supernatant by centrifugation at 1800 g for 20 min, resulting in the precipitation of platelets. The platelet

precipitates were washed twice with PBS, resuspended in water containing a protease cocktail inhibitor, and stored at -80 ℃. Prior to use, the platelets were thawed at room temperature. This freeze-thaw process was repeated three times to ensure uniformity. Finally, the platelet membranes were mixed with TP /NPs to form uniform particles.

Characterization of PM@TP/NPs

The particle size of the TP/NPs was determined using dynamic light scattering (DLS). Surface characteristics of TP/NPs were analyzed via scanning electron microscopy (SEM). Optical properties were assessed using ultraviolet-visible (UV-Vis) spectroscopy. TP/NPs encapsulating platelet membrane proteins were evaluated via SDS-PAGE. Protein samples, including platelet membrane proteins and PM@TP/NPs, were loaded onto a 10% SDS-PAGE gel, followed by staining with Coomassie Blue and imaging after overnight gel decolorization. Additionally, platelet membrane proteins in both platelets and PM@TP/NPs were identified via Western blot using the platelet membrane protein P-selectin (CD62).

Cell culture and nanoparticles uptake

Human bronchial epithelialcells (16HBE, ATCC; Manassas, VA, USA) were cultured in DMEM medium (Gibco, NY, USA), supplemented with 10% fetal bovine serum (FBS, Gibco, USA), 100 U/mL penicillin, and 100 μg/mL streptomycin, and maintained in a humidified atmosphere containing 5% CO_2 at 37℃. To assess nanoparticle uptake, HBE cells were cultured in DMEM with 10% FBS. Following a 24-hour stimulation with 50 μg/mL house dust mite (HDM, Dermatophagoides farina, Greer Laboratories), naked Cou6-TP/NPs or Cou6-PM@TP/NPs were introduced into the culture medium for an additional 2 h. Subsequently, fluorescence microscopy (Olympus IX70 Inverted Microscope) was utilized to capture images of HBE cells. Nanoparticle uptake was quantified using flow cytometry. HBE cells were exposed to either naked Cou6-TP/NPs or Cou6-PM@TP/NPs, then washed twice with PBS to eliminate unbound nanoparticles, and subsequently subjected to trypsinization. Flow cytometry analysis (LSRFortessaTM X-20, BD) was employed for data collection and analysis, with results expressed as the mean fluorescence intensity (MFI) of Cou6 within the cells.

Cell viability assay

A CCK-8 assay was conducted to assess the cell viability of HBE cells. Briefly, HBE cells were seeded at a density of 5×10^3 cells per well in 96-well plates and incubated overnight at 37 °C in a 5% CO2 atmosphere. Subsequently, the culture medium was replaced with varying concentrations of TP, and the cells were further incubated for 24 h at 37 °C. Cell viability was then evaluated using a CCK-8 kit (Beyotime, China) following the manufacturer's protocol.

Hemolysis test

To assess the in vivo biosafety of TP/NPs, a hemolysis test was conducted using red blood cells treated with various formulations of TP nanoparticles [20]. Erythrocytes were obtained from normal C57BL/6J mice by washing anticoagulated whole blood with PBS at 3,500 rpm for 5 min. Subsequently, a 4% red blood cell suspension (v/v in PBS) was mixed with 1 mL of prepared TP and TP nanoparticle solutions (100 μg/mL). After incubating for 4 h at 37 °C, all samples were centrifuged at 3,500 rpm at 4 °C for 5 min to collect the supernatants. The absorbance values (A) of the supernatants from each sample were measured at 550 nm using a microplate reader. The erythrocyte sample lysed with pure water was used as the positive control, while the erythrocyte sample diluted with PBS was used as the negative control. Hemolysis percentage (%) was calculated as follows: Hemolysis (%) = (A sample-A negative control) / (A positive control-A negative control) X100%. Additionally, the red blood cells were added to a 12-well plate and imaged using a live cell imaging system (EVOSFL Auto, Invitrogen, USA) to observe red blood cell morphology.

IVIS imaging

Following the induction of asthma in C57BL/6 mice via HDM exposure, 50 μL of Cou6@TP/NPs (100 μg/mL) and 50 μL of Cou6-PM@TP/NPs (100 μg/mL) were administered intranasally as fluorescent markers, with PBS administration intranasally as the control. Two hours post-administration, images of major mouse organs (heart, lung, liver, spleen and kidney) were captured. Each mouse organ was placed on the scanning platform of the IVIS imaging system to ensure consistent positioning. The PerkinElmer live imaging system was used to capture live fluorescence images of the mice organ. Quantitative analysis was performed using Living Imaging software to assess changes in fluorescence intensity and distribution within the organs.

HDM-induced mouse asthma model

The HDM-induced mouse asthma model used in this study was previously described in our publications [13, 21]. In this experiment, mice were divided into four groups: Basal, HDM, TP, and PM@TP/NPs, with five mice per group. The mouse model of HDM-induced asthma was conducted following this protocol. Eight-week-old female C57BL/6 mice were intranasally sensitized with HDM (200 μg HDM in 50 μL saline per mouse; Mite Dust D. pteronyssinus, Greer Laboratories) on days 0 and 2. On day 14, these mice were intranasally

stimulated challenged with HDM (30 μg in 50 μL saline per mouse) for five consecutive days. Mice in the TP group and the PM@TP/NPs were intranasally administered with TP group or the PM@TP/NPs (10 mg TP per kg body weight) 1 h before HDM stimulation from day 14 to day 21. Normal mice treated intranasally with saline served as the basal control group. Forty-eight hours after the final HDM stimulation on day 21, bronchoalveolar lavage fluid (BALF), sera, and lung tissues were collected for further analysis.

Flow cytometry analysis of bronchoalveolar lavage fluid (BALF) and lung leukocytes

After anesthetizing the mouse, BALF was collected using 5X cold PBS (1 mL) and subjected to flow cytometry analysis. Lung leukocytes were isolated following a previously described method [13]. In brief, lung tissues of mice were minced and digested with 1 mg/mL Collagenase IV (Life Technologies) in RPMI1640 medium containing 5% FBS at 37 °C for 45 min. Subsequently, lung mononuclear cells were isolated using a 38% Percoll gradient (GE Healthcare Life Sciences), and the cells at the bottom of the tube were collected. Red blood cells were lysed using ammonium-chloride-potassium lysis buffer (Life Technologies), and the remaining cells were harvested for flow cytometry analysis.

For flow cytometric examination, cells were surface-stained with antibodies in PBS containing 1% FCS (Sigma-Aldrich) on ice for 30 min. For intracellular cytokine staining, cells were stimulated with 50 ng/mL PMA (Sigma-Aldrich) and 1 μM ionomycin (Sigma-Aldrich) for 5 h in the presence of Golgistop (BD Biosciences). Flow cytometric data were acquired using LSRFortessaTM X-20 and analyzed using FlowJo software (BD Bioscience).

ELISA for the determination of cytokines in sera

Whole blood obtained from mouse heart was centrifuged at 4 ℃ at 5,000 rpm for 10 min. The serum collected from the blood supernatant was used for ELISA analysis. The concentrations of Ig E in BALF and IL-4, IL-5, and IL-13 in mouse serum were measured respectively using ELISA kits (Invitrogen), following the manufacturer's instructions, All samples were measured in duplicate.

Histological analysis

After perfusion with cold PBS, the mouse organs (lung, heart, liver, spleen, and kidney) were fixed in 4% paraformaldehyde (PFA) at room temperature overnight. Subsequently, the organs were embedded in paraffin, sectioned into 5 μm slices, and subjected to hematoxylin and eosin (HE) for analysis.

ROS detection

HBE cells (1×10^6 cells per well) were seeded in 6-well plates and cultured overnight. Following incubation with TP (100 μg/mL) and PM@TP/NPs (100 μg/mL) for 2 h, the cells were stimulated with HDM (100 μg/mL) for 24 h. Subsequently, the cells were treated with DCFH-DA at room temperature for 30 min, following the manufacturer's instructions. After washing the cells twice with PBS, the fluorescence intensity of DCF-HA within the cells was measured using a flow cytometer with a FITC channel. For the detection of reactive oxygen species (ROS) levels in lung tissues, lungs from both normal mice and asthmatic mice were dissected, washed immediately with PBS, and then incubated in DMEM medium containing 100 μM DCFH-DA at 37 °C for 30 min. After washing the lung tissues twice with DMEM, the fluorescence intensity was visualized using a Small Animal Live Imaging System (Eastman Kodak Co, USA).

RT-qPCR

Total RNAs from lung tissues of mice and cells were isolated using TRIzol reagent (Invitrogen) following established protocols [22]. Briefly, 1 μg of total RNA was reverse transcribed into cDNA using the PrimeScript™ RT reagent Kit with gDNA Eraser (TaKaRa) according to the manufacturer's instructions. Quantitative PCR (qPCR) was performed with SYBR Green Master Mix (YEASEN) using The LightCycler® 96 Instrument (Roche, Germany). The relative expression levels were calculated using the comparative Ct value method, with mRNA levels normalized to Gapdh. The primers used for RT-qPCR in this study are listed in Table 1.

Immunoblot analysis

Immunoblot analysis was conducted following established procedures [23]. In brief, Total protein was extracted from cultured HBE cells and lung tissues were lysed with RIPA buffer supplemented with 1% PMSF and a proteinase inhibitor cocktail (Roche, USA) for 30 min on ice. The supernatants were collected by centrifugation at 12,000 g for 20 min. Protein concentrations were determined using a BCA assay. Subsequently, 40 μg of protein samples were separated by 10% SDS-PAGE and electro-transferred onto a PVDF membrane (Millipore, Billerica, USA). The membranes were then blocked and immunoblotted with primary antibodies: P-selectin/CD62p (mouse Ab, Cat No. 60322-1-Ig), HO-1/HMOX1 (rabbit Ab, Cat No. 10701-1-AP), TRL4 (mouse Ab, Cat No.66350-1-Ig), Nrf2 (mouse Ab, Cat No. 66504-1-Ig) from Proteintech Inc. USA; p-Erk1/2 (rabbit Ab, Cat No. 4370), p-P38 (rabbit Ab, Cat No. 4511), P65 (mouse Ab, Cat No. 8242), and GAPDH (rabbit Ab, Cat No.2118) from Cell Signaling Technology Inc. USA. Finally, the blots were visualized using enhanced chemiluminescent

Table 1 List of primers used for RT-qPCR

Gene Mouse	Forward primer	Reverse primer
Il4	GGTCTCAACCCCCAGCTAGT	GCCGATGATCTCTCTCAAGTGAT
Il5	CTCTGTTGACAAGCAATGAGACG	TCTTCAGTATGTCTAGCCCCTG
Il13	CCTGGCTCTTGCTGCCTT	GGTCTTGTGTGATGTTGCTCA
Il6	ATGAAGTTCCTCTCTGCAAGAGACT	CACTAGGTTTGCCGAGTAGATCTC
Tnfa	CAGGCGGTGCCTATGTCTC	CGATCACCCCGAAGTTCAGTAG
Ccl2	TTAAAAACCTGGATCGGAACCAA	GCATTAGCTTCAGATTTACGGGT
Ccl20	AAGACAGATGGCCGATGAAG	AGGTTCACAGCCCTTTTCAC
Il25	ACAGGGACTTGAATCGGGTC	TGGTAAAGTGGGACGGAGTTG
Muc5ac	GGACTTCAATATCCAGCTACGC	CAGCTCAACAACTAGGCCATC
Muc5b	GCCGAGGCAAGTACCTGTC	ACAGCCCTTATACCGCAAGAC
Gapdh	AGGTCGGTGTGAACGGATTTG	TGTAGACCATGTAGTTGAGGTCA
Human		
Ccl2	ATGAAAGTCTCTGCCGCCCT	GGCATTGATTGCATCTGGCTG
Ccl20	CAAGAGTTTGCTCCTGGCTGCTGC	AGTCAAAGTTGCTTGCTTCTGAT
Il25	CCCCCTGGAGATATGAGTTGG	GAGCCTGTCTGTAGGCTGAC
Gapdh	ACAACTTTGGTATCGTGGAAGG	GCCATCACGCCACAGTTTC

reagents (Millipore) and imaged with an AI600 software (GE Healthcare, USA).

Statistical analysis

Statistical analysis was conducted using GraphPad Prism 8 and IBM SPSS Statistics 22 software. Comparison of the variables between groups was made by student's t-test or one-way ANOVA followed by Tukey's post-hoc test. $P<0.05$ was considered for the statistical significance. All results represent mean ± standard deviation (SD).

Results

Synthesis and characterization of PM@TP/NPs

The PM@TP/NPs nanoparticles were prepared following our previously reported method [13]. Briefly, Tea polyphenols were loaded onto PLGA-PEG nanoparticles using the double emulsion method to form TP@NPs. Subsequently, platelet membranes were obtained through repeated freeze-thaw cycles and used to prepare PM@TP/NPs. After formulating the PM@TP/NPs, their size distribution and morphology were characterized by dynamic light scattering (DLS) and scanning electron microscopy (SEM) respectively, before and after wrapping with the platelet membrane. The mean size distribution of TP/NPs increased from approximately 239 nm to 425 nm after cloaking with the platelet membrane (Fig. 1A), indicating successful acquisition of PM@TP/NPs. SEM images (Fig. 1B) revealed a thick membrane layer after coating with the platelet membrane, with PM@TP/NPs displaying a spherical shape with a diameter of around 425 nm. The loading capacity of TP into NPs was assessed using UV-Visible Spectrometry. The optical characterization of TP/NPs (Fig. 1C) exhibited a maximum UV-Vis absorption at around 200 nm. PM@TP/NPs displayed an absorption spectrum very similar to free TP, suggesting successful encapsulation of TP into the PM@TP/NPs. Furthermore, the presence of platelet membrane protein in PM@TP/NPs was validated using SDS-PAGE (Fig. 1D), confirming the preservation of characteristic membrane proteins such as the platelet membrane protein P-selectin (CD62). Additionally, platelet membrane proteins were further confirmed by Western blot using a P-selectin antibody. Overall, these results demonstrate the successful conjugation or coating of platelet membranes on the surface of the nanoparticles.

Bioavailability, biosafety and biocompatibility evaluation of the TP/NPs

Due to its susceptibility to oxidation and subsequent loss of activity, the bioavailability of free TP was evaluated through a storage experiment. Over several weeks of water dissolution, the color of TP solution turned yellow, indicative of oxidation (Fig. 2A). Additionally, precipitation occurred after one week of TP storage in water, contrasting with the orange color of TP/NP solution and the absence of precipitation (Fig. 2A), indicating uniform dispersion of TP/NPs in water. Given the pivotal role of nanoparticle biosafety in clinical therapy, the cell viability of TP in HBE cells was assessed using a CCK8 test kit. As displayed in Fig. 2B, TP concentrations below 128 μg/mL exhibited excellent cell viability in HBE cells, suggesting this as the safe range between 0 and 128 μg/mL of TP concentration for treatment in vitro. Based on our previously results [24], a concentration of 100 μg/mL of TP and its nanoparticles was selected for in vitro experiments in this study.

To evaluate TP's biosafety in vivo, HDM-induced asthmatic mice were intranasally administered TP (10 mg/kg) and PM@TP/NPs (10 mg/kg). H&E staining (Fig. 2C) revealed no evident lesions in major organs (heart, liver,

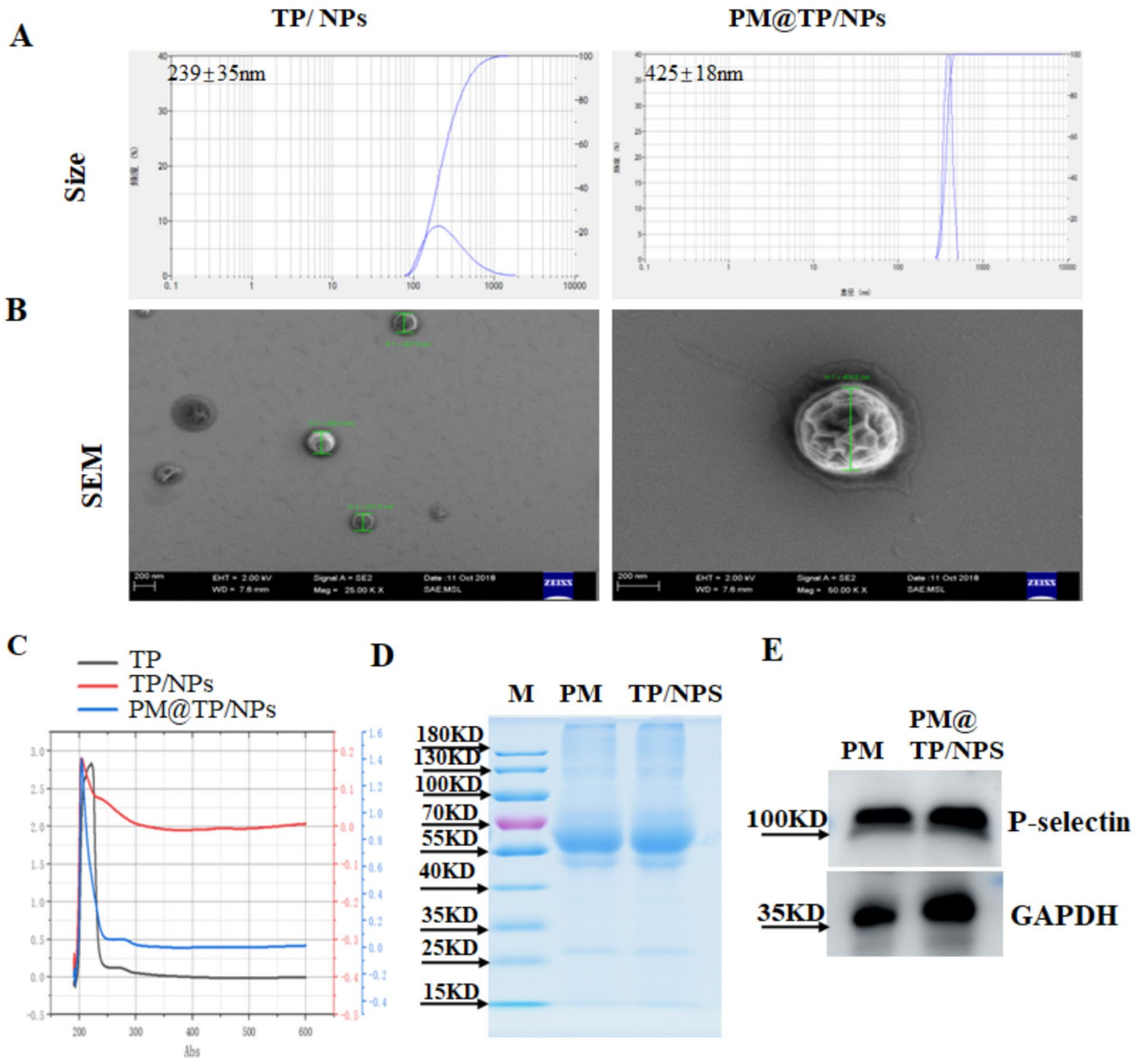

Fig. 1 Synthesis and characterization of PM@TP/NPs. (**A**) Mean size of TP-NPs and PM@TP/NPs were measured by. Dynamic Light Scattering (DLS) analyzers ($n = 3$). (**B**) Scanning electron microscope (SEM) image of TP/NPs and PM@TP/NPs. Scale bar = 100 nm, $n = 3$. (**C**) The encapsulation of TP was detected using an ultraviolet and visible spectrophotometer (UV6000). (**D**) Proteins of platelet membrane (PM) and PM@TP/NPs were analyzed by SDS-PAGE. (**E**) Proteins of platelet membrane and PM@TP/NPs were confirmed by Western blot with P-selectin antibody, GAPDH as a reference

spleen, and kidney) of the PM@TP/NPs group at a concentration of 100 mg/kg. Furthermore, to confirm TP's biocompatibility in vivo, hemolytic properties of TP and its modified nanoparticles were assessed by erythrocyte hemolysis assay. Both TP and its nanoparticles were tested at a concentration of 100 μg/mL (calculated based on the TP loading into NPs). While TP showed slight hemolysis (Fig. 2D), TP nanoparticles significantly reduced hemolysis compared to free TP, with PM@TP/NPs demonstrating the most pronounced effect. Optical microscope images of erythrocytes treated with TP and its nanoparticles (Fig. 2E) further supported these findings, revealing reduced cell lysis with nanoparticle treatment compared to free TP. Notably, PM@TP/NPs exhibited superior efficacy in improving red blood cell survival rates compared to TP/NPs, underscoring the potential of biomimetic nanoparticles coated with platelet membrane to enhance drug biocompatibility in vivo. Collectively, these findings highlight the significant enhancement of TP biocompatibility and biosafety achieved with PM@TP/NPs.

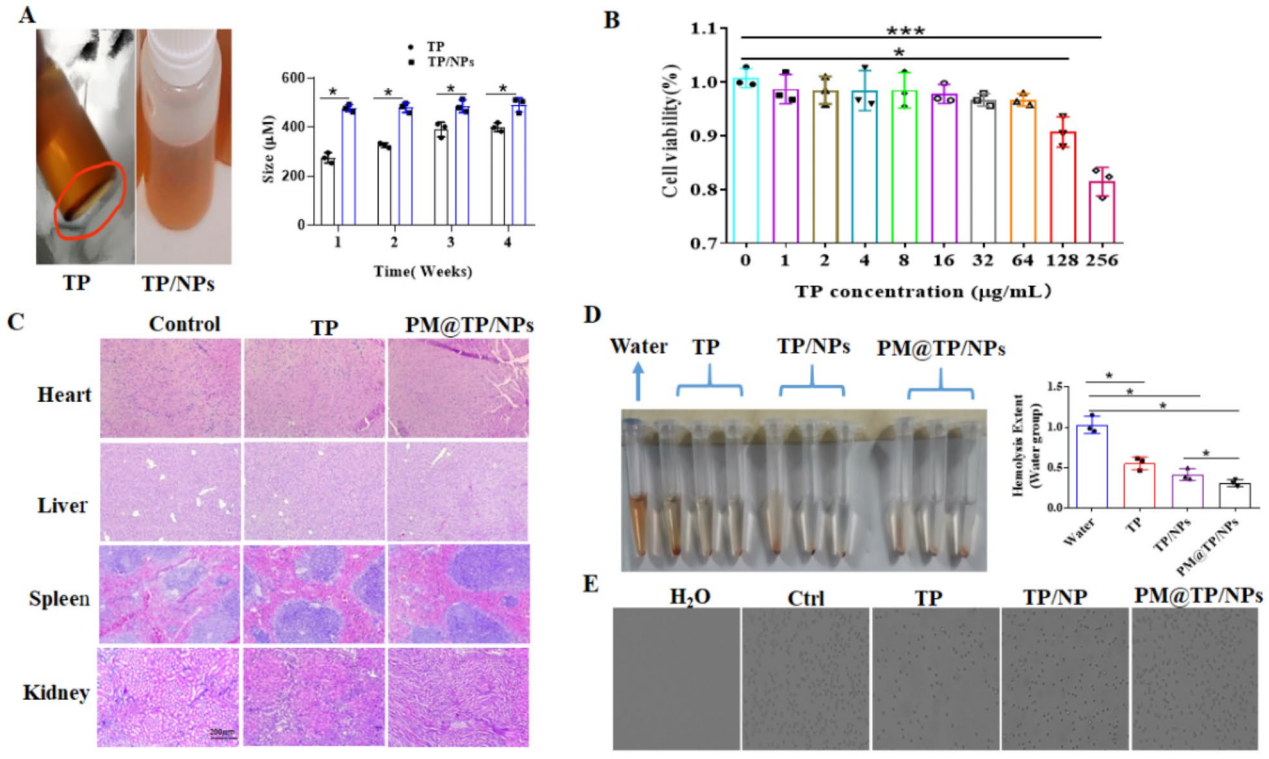

Fig. 2 Bioavailability, biosafety and biocompatibility evaluation of the NPs. (**A**) Bioavailability of TP and TP/NPs were tested in different storage times by storage experiment ($n=3$). *$p<0.05$ *versus* free TP group. (**B**) HBE cells were treated with various concentration of TP ranging from 0 to 256 μg/mL for 24 h, cell viability was determined using the CCK8 assay ($n=3$). *$p<0.05$, ***$P<0.001$ *versus* the untreated control group. (**C**) After 100 mg/kg TP and PM@TP/NPs were administered intranasally to mice, mouse major organs (heart, liver, spleen and kidney) were evaluated by H&E staining. Intranasal administration of PBS as a control ($n=3$). Bar: 200 μm. (**D-E**) The images of hemolysis assay of pure water, free TP, TP/NPs and PM@TP/NPs, separately. The morphology of erythrocytes treated with free TP, TP/NPs, and PM@TP/NPs separately by light microscope ($n=3$). *$p<0.05$ *versus* water group and PM@TP/NPs group

PM@TP/NPs reduced HDM-induced inflammation in HBE cells by suppressing ROS production and the CCL2/ MAPK signaling pathway

To understand how to scavenge ROS in HDM-induced airway epithelial inflammation with TP treatment, we assessed ROS production, the expression levels of ROS-associated proinflammatory cytokines and chemokines, and the MAPK signaling pathway in HBE cells following HDM stimulation. Following treatment with TP and HDM, HBE cells were stained with DCFH-DA and analyzed by flow cytometry. Notably, PM@TP/NPs demonstrated significant inhibition of ROS production in HDM-challenged HBE cells compared to other treatment groups (Fig. 3A-B). Additionally, we evaluated the mRNA expression levels of *Ccl2*, *Ccl20*, and *Il25* using real-time qPCR (Fig. 3C). The results revealed that PM@TP/NPs markedly decreased the mRNA expression of *Ccl2* compared to TP treatment following HDM stimulation. However, there were no significant differences observed in the mRNA expressions of *Ccl20* and *Il25* among all treatment groups. The results indicated that PM@TP/NPs effectively suppressed Erk1/2 and P38 signaling pathways following HDM stimulation (Fig. 3D). These findings suggest that PM@TP/NPs alleviate HDM-induced inflammation in HBE cells by attenuating ROS production and modulating the CCL2/MAPK signaling pathway.

The coating of platelet membrane promoted inflammation targeting and facilitated TP accumulation

To improve the precision targeting of NPs, the platelet membrane was coated to facilitate the inflammation targeting of NPs. To examine the targeting efficacy of TP/NPs, coumarin 6 (Cou6) was co-encapsulated into the TP/NPs (Cou6-PM@TP/NPs) as the fluorescent marker. The mean fluorescence intensity (MFI) of Cou6-TP/NPs and Cou6-PM@TP/NPs were determined by microscope and flow cytometry to evaluate cell uptake. HBE cells were treated with TP/NP and PM@TP/NPs for 1 h under conditions stimulated by PBS and HDM. The results in Fig. 4A indicated no significant difference in TP/NPs uptake in PBS-treated HBE cells compared to PM@TP/NPs. However, in HDM-induced inflammatory HBE cells, PM@TP/NPs exhibited significantly increased cell uptake. Flow cytometry confirmed higher MFI values for PM@TP/NPs in HBE cells compared to naked TP/NPs after HDM stimulation (Fig. 4B and C). These

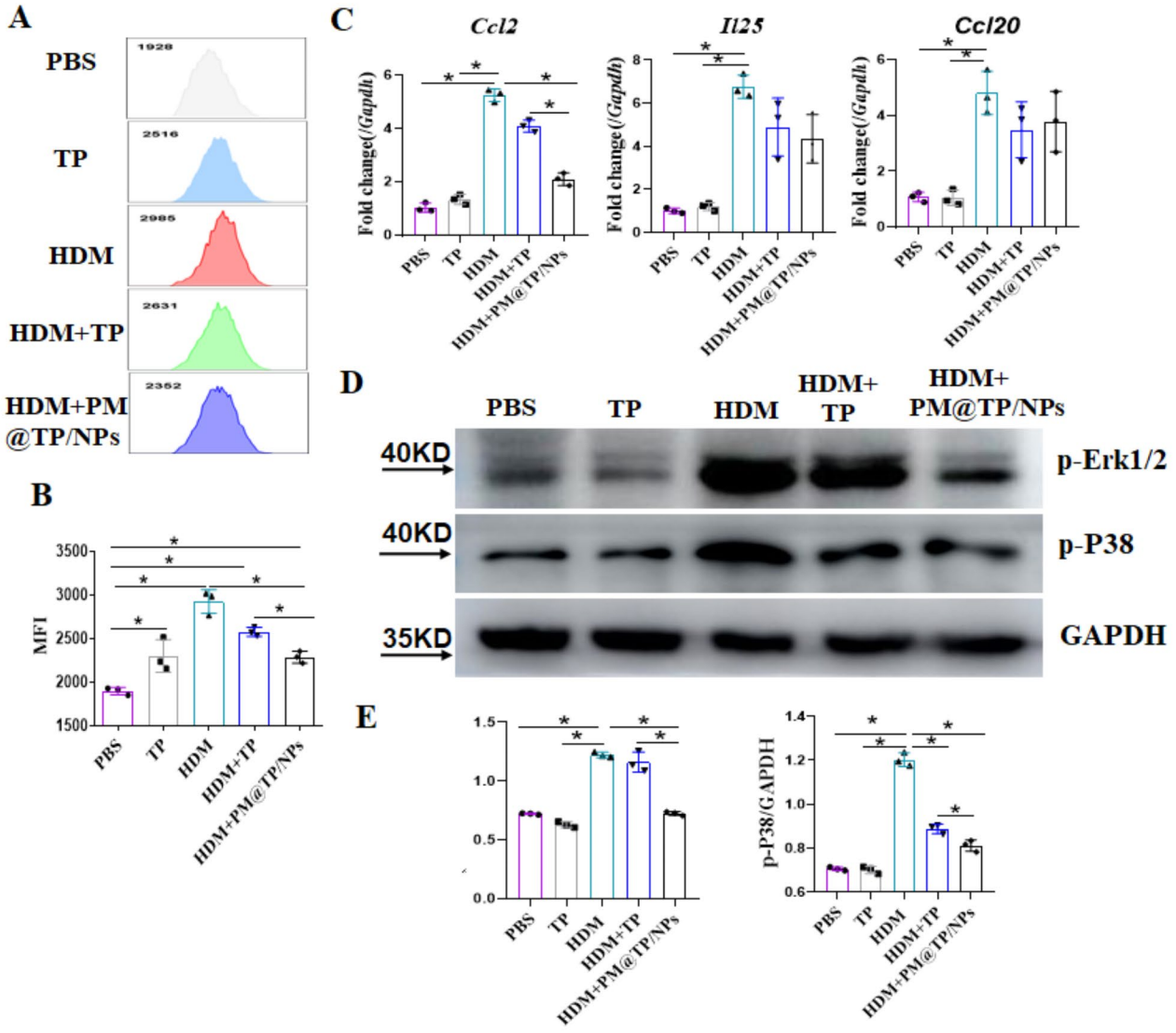

Fig. 3 PM@TP/NPs reduced HDM-induced inflammation in HBE cells by suppressing ROS production and CCL2/ MAPK signaling pathway. (**A**) HBE cells pretreated with different formulations of TP (100 μg/mL) for 3 h before 100 μg/mL of HDM challenging, then HBE cells with different treatments were stained with DCF-HA kits. The reactive oxygen species (ROS) level of 20,000 cells was determined by flow cytometry, and (**B**) the mean fluorescent intensity (MFI) of HBE cells was measured by flowjo software. (**C**) The mRNA expression of *Ccl2*, *Il25*, and *Ccl20* in HBE cells after HDM (100 μg/mL) stimulation was determined by RT-qPCR ($n=3$). (**D-E**) Western blot was used to examined Erk1/2、P38 signal pathways in HBE cells treated with different formulations of TP ($n=3$). *$p<0.05$

observations imply that PM@TP/NPs predominantly taken up by inflammatory bronchial epithelial cells, showcasing excellent targeting ability *in vitro.*

To further assess the targeting and accumulation of PM@TP/NPs in inflammatory lungs, various organs of HDM-induced asthmatic mice were imaged using an IVIS imaging system. The targeting capabilities of Cou6-TP/NPs and Cou6-PM@TP/NPs against inflammatory lungs were evaluated by in vivo imaging of fluorescent mice. Strong fluorescence signals were observed in mouse lung tissues 2 h after i.n. administration of TP nanoparticles, indicating enhanced targeting ability (Fig. 4D). Additionally, statistical analysis of MFI demonstrated higher fluorescence intensity in mouse lungs for the Cou6-PM@TP/NPs group compared to the Cou6-TP/NPs group, suggesting superior inflammatory targeting ability for PM@TP/NPs. These results indicate that Cou6-PM@TP/NPs significantly contribute to improved drug delivery and accumulation in inflammatory lungs.

PM@TP-NPs enhanced the attenuation of airway inflammatory cell infiltration in HDM-induced asthma

To explore the therapeutic potential of PM@TP/NPs as an antioxidant agent in mice, we assessed the efficacy of

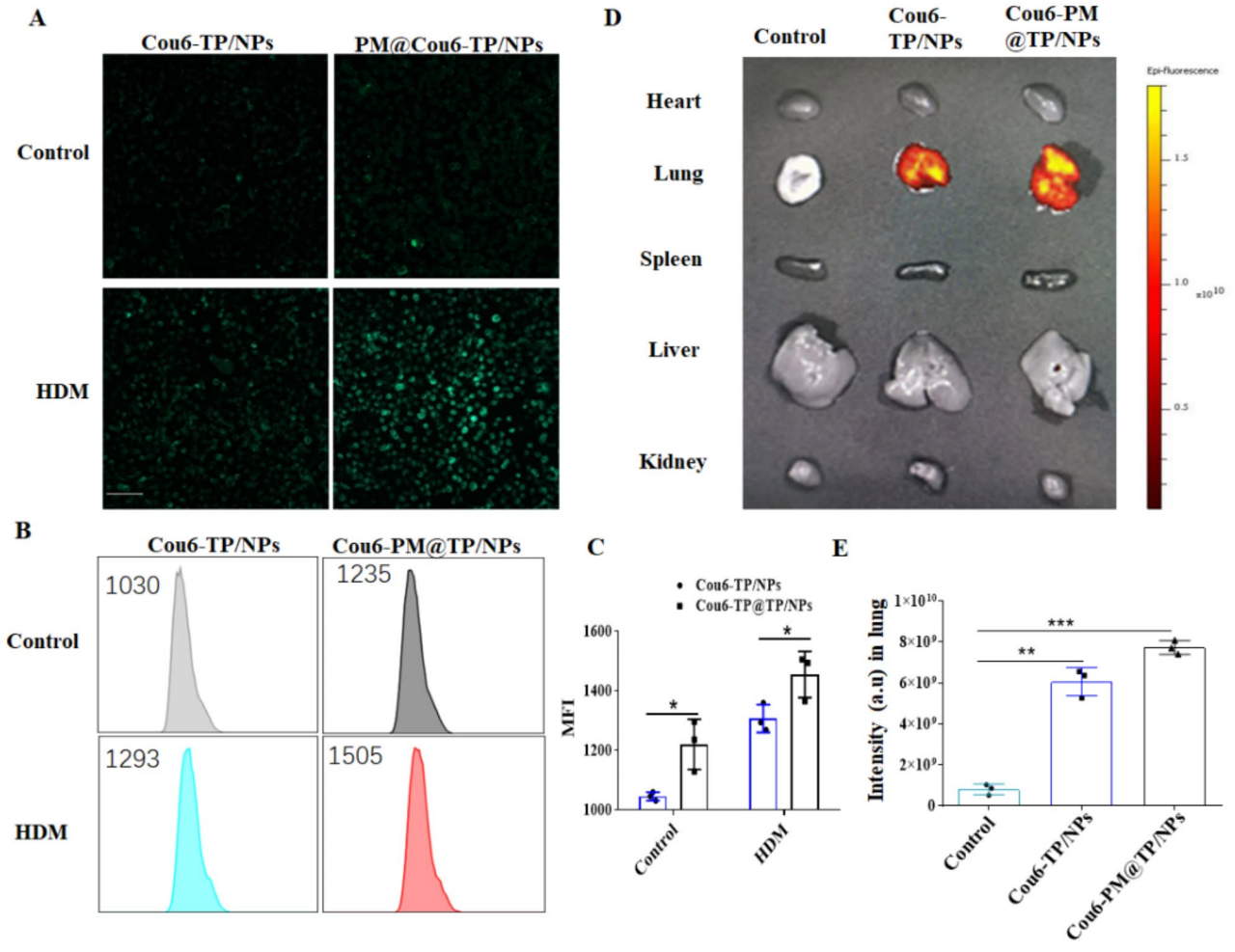

Fig. 4 The coating of platelet membrane promoted inflammation targeting and facilitated TP accumulation. (**A**) Cou6 was encapsulated into the NPs as a fluorescence marker. The intracellular uptake of Cou6-TP/NPs and Cou6-PM@ TP/NPs in HBE cells with or without HDM treatment, was observed using a fluorescence microscope ($n=3$). (**B-C**) The typical images and the fluorescence intensity in HBE cells co-cultured with Cou6-TP/NPs and Cou6-PM@TP/NPs with or without HDM treatment by flow cytometry ($n=3$). *$p<0.05$ *versus* control group. (**D-E**) Biodistribution and retention of PM@blank-TP/NPs, naked Cou6-TP/NPs, and Cou6-PM@TP/NPs in mouse major organs determined by IVIS imaging system at 2 h after NP intranasal administration ($n=4$). **$p<0.01$; ***$p<0.001$ *versus* control group

TP and its NPs in alleviating eosinophilic airway inflammation in an HDM-induced asthma model. As depicted in Fig. 5A, asthmatic mice exhibited significantly higher levels of infiltrated leukocytes compared to normal mice (Basal group). Both TP and the biomimetic NPs demonstrated a reduction in infiltrated leukocytes in the bronchoalveolar lavage fluid (BALF) of asthmatic mice. Notably, PM@TP/NPs exhibited a greater reduction in inflammatory cell infiltration into the mouse airways compared to TP treatment alone. Additionally, PM@TP/NPs significantly decreased total eosinophil numbers while increasing macrophage numbers in BALF. However, PM@TP-NPs did not affect total neutrophil and lymphocyte numbers in BALF (Fig. 5B and C).

Furthermore, asthmatic mice exhibited elevated levels of IgE in sera and Th2-associated proinflammatory cytokines such as IL-4, IL-5, and IL-13 concentrations in BALF compared to normal mice. Both TP and its NPs reduced IgE levels in sera and secretion of proinflammatory cytokines (Fig. 5D). Importantly, PM@TP/NPs demonstrated a greater reduction in IgE levels in sera and secretion of proinflammatory cytokines in BALF compared to TP treatment alone (Fig. 5D). These findings collectively indicate that PM@TP/NPs significantly enhanced the reduction of airway inflammation in the HDM-induced mouse asthma model, suggesting their potential as an effective therapeutic approach for asthma.

PM@TP/NPs relieved pulmonary inflammation in asthmatic mice

To further investigate the therapeutic potential of TP and its biomimetic NPs in mitigating pulmonary

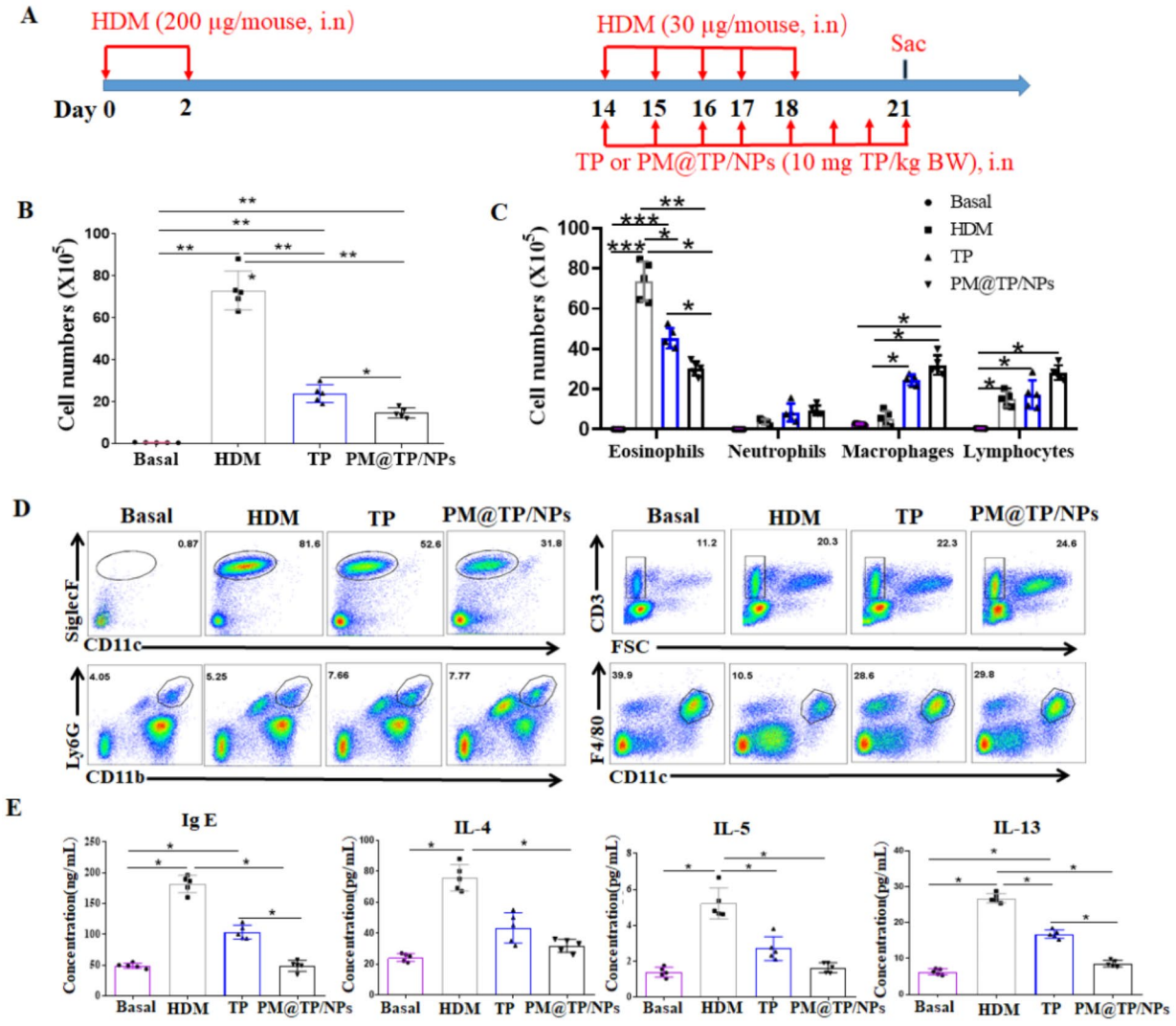

Fig. 5 PM@TP-NPs enhanced the attenuation of airway inflammatory cell infiltration in HDM-induced asthma. (**A**) Experimental scheme for HDM-induced mouse model of asthma. Eight-week-old C57BL/6 female mice ($n = 5$ per group) were subjected to a HDM-induced asthma model. Mice were intranasally sensitized with HDM (200 μg HDM in 50 μL saline per mouse) on days 0 and 2. Subsequently, these mice were intranasally stimulated with HDM (30 μg in 50 μL saline per mouse) on day 14 for five consecutive days. The TP group and the PM@TP/NPs group of mice were intranasally administered (10 mg TP per kg body weight) 1 h before HDM stimulation from day 14 to day 21. Normal mice treated intranasally with saline served as the basal control group in this experiment. Forty-eight hours after the final HDM stimulation on day 21, Bronchiolar alveolar lavage fluid (BALF), sera, and lung tissues were collected. (**B-C**) Two days after the last stimulation, total cell counts, eosinophils, neutrophils, macrophages, and lymphocyte cells in the BALF of mice were quantified by flow cytometry. (**D**) Representative BALF cells were prepared by flow cytometry analysis. (**E**) IgE levels in sera and the content of proinflammatory factors (IL-4, IL-5, and IL-13) in BALF were quantified by ELISA. $^{*}p < 0.05$, $^{**}p < 0.01$, $^{***}P < 0.001$

inflammation in HDM-induced asthmatic mice, lung mononuclear cells were isolated from asthmatic mice using collagenase digestion for flow cytometry analysis. Asthmatic mice exhibited higher total leukocyte and eosinophil numbers in the lungs compared to normal mice. However, TP and its NPs reduced these numbers more effectively than PBS treatment alone (Fig. 6A-C). Notably, PM@TP/NPs demonstrated superior therapeutic effects in reducing lung inflammatory cells compared to TP alone. Histological examination with H&E staining revealed that PM@TP/NPs improved the reduction of leukocyte infiltration in the lungs of mice (Fig. 6D). Furthermore, mRNA expressions of proinflammatory cytokines and mucin in the lungs of asthmatic mice were determined by RT-qPCR. The results showed a significant increase in gene expression in the lungs of asthmatic mice compared to normal mice. PM@TP/NPs notably inhibited the expression of Th2-type cytokines (*Il5*, *Il13*) and mucin gene *(Muc5c*), while showing no effects on other proinflammatory cytokines (*Il4*, *Tnf*, *Il6*, and *Ifnγ*) and mucin gene (*Muc5ab*) (Fig. 6E).

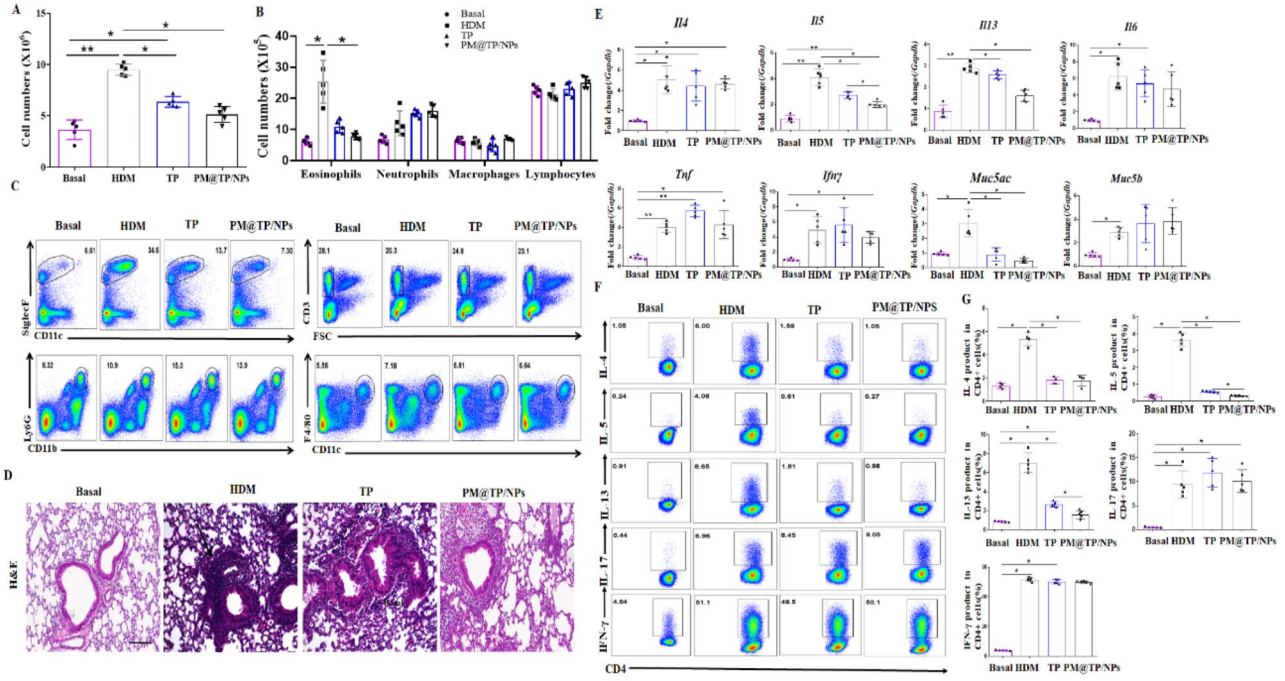

Fig. 6 PM@TP/NPs relieved lung inflammation in asthmatic mice. (**A-B**) Infiltrated cells in the lung with normal mice and HDM-induced asthmatic mice ($n=5$ per group) were isolated and total cell counts, eosinophils, neutrophils, macrophages and lymphocyte cells in the lung were calculated by flow cytometry. (**C**) Representative lung inflammatory cells were prepared by flow cytometry analysis. (D) Representative micrographs of lung tissue cross-sections from mice with normal mice and HDM-induced asthma were stained by H&E ($n=3$). Bars: 100 μm. (**E**) The mRNA expression of pro-inflammatory cytokines from normal mice and HDM-induced asthmatic mice ($n=5$ per group) with or without treatment was examined by RT-qPCR. (**F-G**) Th-producing cells in the lungs from normal mice and HDM-induced asthmatic mice ($n=5$ per group) were isolated and followed by flow cytometry analysis. $^{*}p<0.05$; $^{**}p<0.01$

Additionally, Th cell production in the lungs of HDM-induced asthmatic mice was examined by flow cytometry. Asthmatic mice exhibited higher levels of IL-4, IL-5, and IL-13-producing Th2 cells, IFNγ-producing Th1 cells, and IL-17-producing Th17 cells in the lungs compared to normal mice. However, the PM@TP/NPs group showed a greater decrease compared to the TP group, with no significant difference observed in IFNγ-producing Th1 cells and IL-17-producing Th17 cells among all groups (Fig. 6F and G). Taken together, this evidence demonstrates that PM@TP/NPs can significantly alleviate lung inflammation. Therefore, inhaled administration of PM@TP/NPs as an antioxidant agent may represent a novel potential therapeutic strategy for treating asthma.

PM@TP/NPs enhanced ROS scavenging capacity, activated the Nrf2/HO-1 signaling pathway, and suppressed the Ccl2/MAPK and TLR4/NF-κB signaling pathways in asthmatic mice

To investigate whether PM@TP/NPs alleviate lung inflammation in HDM-induced asthma by scavenging ROS production, we initially assessed ROS levels in asthmatic mice. The ROS scavenging ability of TP was evaluated using DCFH-DA. As shown in Fig. 7A, asthmatic mice exhibited elevated ROS levels in the lungs compared to normal mice during HDM-induced asthma. However, the PM@TP/NPs group demonstrated a significant reduction in ROS production compared to the TP group. These findings indicate that PM@TP/NPs possess enhanced ROS scavenging capability in vivo compared to free TP.

As we explored TP's role in scavenging ROS in HDM-induced asthma, we also analyzed the expression of proinflammatory cytokines and chemokines secreted by epithelial cells, along with potential MAPK signaling pathways associated with ROS production, using RT-qPCR and Western blot analysis. As depicted in Fig. 7B, gene expression of *Ccl2* and *Il25* in the lungs of asthmatic mice was markedly elevated compared to normal mice. However, PM@TP/NPs significantly reduced the gene expression of *Ccl2* and *Il25* in the lungs of asthmatic mice compared to TP, with no effect on the mRNA expression of *Ccl20*. Additionally, MAPK signaling pathways such as Erk1/2 and P38 were activated in the lungs of asthmatic mice compared to normal mice. Nonetheless, PM@TP/NPs remarkably suppressed Erk1/2 and P38 signaling pathways in the lungs of asthmatic mice (Fig. 7C). Furthermore, recent studies have shown that TPs can alleviate lung inflammation by activating the Nrf2/HO-1 signaling pathway [25] and deactivating the TLR4/NF-κB

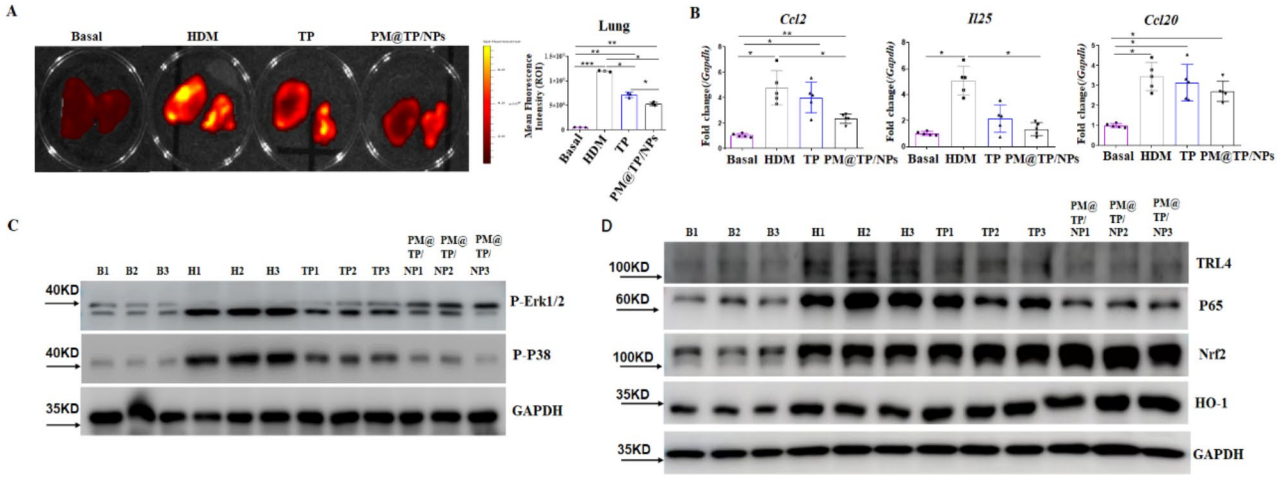

Fig. 7 PM@TP/NPs enhanced ROS scavenging capacity, activated the Nrf2/HO-1 signaling pathway, and suppressed the Ccl2/MAPK and TLR4/NF-κB signaling pathways in asthmatic mice. (**A**) Representative micrographs of lung tissues of normal mice and the mice with different TP treatments (100 μg/mL) ($n = 3$ per group) were stained with DCF-HA kits and determined by an IVIS imaging system. Relative fluorescence intensity of in lungs (ROS levels) originated from normal mice (Basal group) and HDM-induced asthmatic mice treated with PBS, TP or PM@TP/NP were analyzed by IVIS imaging system. *$p < 0.05$, **$p < 0.01$, *** $P < 0.001$. (**B**) The mRNA expression of *Ccl2*, *Il25* and *Ccl20* in the lung of mice in the basal group) and asthmatic mice ($n = 5$ per group) were detected by real-time qPCR. *$p < 0.05$, **$p < 0.01$ *versus* Basal. *$p < 0.05$ *versus* PM@TP/NPs. (**C**) Erk1/2 and P38 signal pathways were examined in the lung of mice in the basal group and asthmatic mice with different TP treatments by Western blot ($n = 3$ per group). (**D**) TLR4/NF-κB signal pathways and Nrf2/HO-1 signal pathways were examined in the lung of mice in the basal group and asthmatic mice treated with different TP formulations using Western blot analysis ($n = 3$ per group)

signaling pathway [26]. The results also were confirmed by western blot in the lungs of asthmatic mice (Fig. 7D). Overall, these results suggest that PM@TP/NPs enhance antioxidant activity and therapeutic efficacy in asthma through improving ROS scavenging capacity while concurrently activing Nrf2/HO-1 signaling pathway and suppressing the *Ccl2*/MAPK and TLR4/NF-κB signaling pathway in the lungs of asthmatic mice. These findings align with observations from HDM-induced inflammation in HBE cells treated with PM@TP/NPs. Thus, all of these results illustrate that PM@TP/NPs potentially attenuate asthma by scavenging ROS and concurrently activing Nrf2/HO-1 signaling pathway while suppressing the *Ccl2*/MAPK and TLR4/NF-κB signaling pathway.

Discussion

In recent decades, inhalation or systemic administration of glucocorticosteroids has been the primary clinical approach for treating asthma. However, their long-term use or administration at high doses often brings about significant adverse effects on the human body [27]. In response to this challenge, numerous studies including Chinese herbal medicine have demonstrated to ameliorate asthma by scavenging ROS production [28, 29]. Tea polyphenols have demonstrated potent ROS scavenging abilities and have been explored as potential candidates for novel antioxidant or anti-inflammatory drugs [30, 31]. However, the limited bioavailability and biocompatibility of tea polyphenols have hampered their clinical efficacy.

Numerous studies have indicated that exposure to nanoparticles can contribute to the development and exacerbation of asthma due to their toxic effects. However, most of these nanoparticles originate from sources such as carbon nanotubes, carbon-based nanoparticles, and metal oxide nanoparticles [32]. In our experiments, we chose to employ PLGA due to its lower immunogenicity and non-toxicity to lung tissues. PLGA is a biodegradable functional polymer organic compound known for its excellent biocompatibility, non-toxicity, and efficient encapsulation properties. Additionally, when modified with polyethylene glycol (PEG), PLGA nanocarriers exhibit prolonged circulation time in the body and significantly enhanced passive targeting of inflammatory organs [33]. Recently, carriers modified with cell membranes, which possess characteristics such as prolonged circulation time, excellent biocompatibility, and strong targeting capabilities, have gained widespread use in the treatment of pulmonary inflammatory diseases [34]. Platelet membrane-coated nanoparticles have garnered significant attention due to the unique properties of platelets, including immune evasion, sub-endothelial adhesion, and interactions with pathogens [35, 36]. Consequently, various platelet membrane-coated nanoparticles have been developed for targeted drug delivery to tumors and inflammatory diseases [12, 37]. Our previous studies have demonstrated the benefits of platelet membrane coating in the treatment of pulmonary inflammation, including asthma [13], and septic pneumonia [38], owing to its remarkable inflammation-targeting ability.

In this study, our platelet membrane-coated tea polyphenol nanoparticles (PM@TP/NPs) exhibited excellent characteristics in terms of nanoparticle size distribution and demonstrated significantly improved bioavailability, biosafety, and biocompatibility compared to free tea polyphenols (TP). Furthermore, PM@TP/NPs showed enhanced cellular uptake in vitro and targeted lung tissues within the inflammatory microenvironment more effectively than TP and TP/NPs alone. In an HDM-induced asthma model, PM@TP/NPs markedly attenuated pulmonary inflammation in mice, as evidenced by reduced eosinophil infiltration and expression of Th2 proinflammatory cytokines compared to free TP treatment. These results suggest that inhaled administration of PM@TP/NPs not only improves their biocompatibility and enhances their stability in vivo, but also effectively alleviates asthma as an antioxidant agent.

Airway epithelial cells, associated with ROS activation, represent an initial step in asthma pathogenesis and are often accompanied by processes such as airway remodeling and secretion of pro-inflammatory factors [39]. Inflammatory cytokines and chemokines secreted by epithelial cells, such as CCL2, CCL20, and IL-25, play a crucial role in ROS generation [40–42]. Tea polyphenols have been shown to effectively scavenge ROS as potent antioxidants and suppress inflammatory cytokine secretion by regulating various intracellular signaling cascades [43, 44]. Therefore, we investigated the mRNA expression of *Ccl2*, *Ccl20*, and *Il25* in HDM-induced epithelial cells and asthmatic mice following TP treatment. The results revealed that PM@TP/NPs significantly reduced CCL2 mRNA expression, thus attenuating inflammation in both cells and asthmatic mice. Previous studies have shown that TPs can alleviate allergen-induced asthma by activating the Nrf2/HO-1 signaling pathway [26] and deactivating the TLR4/NF-κB signaling pathway [27]. The results also were confirmed by western blot in HDM induced asthmatic mice this study. Furthermore, recent several studies have highlighted the critical role of the MAPK signaling pathway in ROS generation [45, 46]. Therefore, we also examined the expression changes in MAPK pathways, such as Erk and P38, in both HDM-induced cells and asthmatic mice by western blot following TP treatment. Our results demonstrated that PM@TP/NPs inhibited the expression of Erk and P38 signal pathways in both cells and asthmatic mice. These findings collectively illustrate that the potential mechanism underlying the therapeutic efficacy of PM@TP/NPs in asthma involves the reduction of ROS production, suppression of CCL2 expression, and inhibition of the MAPK signaling pathway. This underscores the promising application of PM@TP/NPs for asthma treatment as a ROS-responsive nanoparticles.

Conclusions

In this study, we successfully designed platelet membrane-cloaked nanoplatform to deliver TPs for asthma treatment. The synthesized PM@TP/NPs exhibited excellent dispersion, good biocompatibility, and biosafety both in vitro and in vivo. These PM@TP/NPs effectively evaded immune system clearance and successfully accumulated in the inflamed lungs of asthmatic mice. We investigated the therapeutic potential of PM@TP/NPs as a novel antioxidant agent for alleviating HDM-induced asthma. Through in vitro cell experiments and in vivo mouse studies, we demonstrated that PM@TP/NPs effectively reduced ROS production by reducing CCL2 expression and inhibiting the MAPK signaling pathway. Notably, inhaled administration of PM@TP/NPs significantly attenuated inflammation and alleviated oxidative stress-induced lung inflammation in HDM-induced mouse asthma.

Recently, numerous studies have demonstrated that TPs act as potent antioxidants for treating respiratory diseases such as asthma, chronic obstructive pulmonary disease, and lung fibrosis. Furthermore, TPs serve as novel neuroprotective agents for neurodegenerative diseases and as anti-tumor agents for cancer treatment. The platelet membrane-cloaked nanoplatform overcomes the limitations of TPs' low biocompatibility and potential toxicity, enhancing their stability and bioavailability within living organisms. Taken together, our findings suggest PM@TP/NPs have promising efficacy in the treatment of asthma and could potentially be used to treat other diseases in clinical application by targeting ROS production scavenging in the future.

Supplementary Information

The online version contains supplementary material available at https://doi.org/10.1186/s12931-024-02947-3.

Supplementary Material 1

Author contributions

SO and GH wrote the manuscript text and supervised the project. SO, HJ, JL, WW, RL and BW preprared Figs. 1, 2 and 3 and SO, PL, JL and WW preprared Figs. 4, 5, 6 and 7. XH and XL reviewed the manuscript and provided resources for the work. All authors have reviewed the manuscript.

Funding

This work was supported by the National Natural Science Foundation of China (82370039, 82001702), Guangdong Basic and Applied Basic Research Foundation (2021B1515130004, 2022A1515140075, 2021B1515140021, 2022A1515140062), Scientific research project of Traditional Chinese Medicine Bureau of Guangdong Province (20221412), Medical Research Foundation of Guangdong Province (B2023056), the Science Foundation of Dongguan Science and Technology Bureau (20211800905022, 20231800940452, 20231800940112), The Two Universities' Paired and Cooperated Research Team Project of Guangdong Medical University (4SG22261G) .

Data availability

No datasets were generated or analysed during the current study.

Declarations

Ethics approval and consent to participate
All the experiments in this study were performed in accordance with relevant guidelines and regulations of Animal Ethics Committee of Guangdong Province, China. Animals and animal protocol were approved by The Institutional Animal Care and Use Committee of Guangdong Medical University (Approved number: GDY2002326)).

Consent for publication
Not applicable.

Competing interests
The authors declare no competing interests.

Received: 12 May 2024 / Accepted: 8 August 2024
Published online: 17 August 2024

References

1. Oz HS, Chen T, de Villiers WJ. Green Tea polyphenols and sulfasalazine have parallel anti-inflammatory properties in colitis models. Front Immunol. 2013;4:132.
2. Fernandes L, Cardim-Pires TR, Foguel D, Palhano FL. Green Tea Polyphenol. Epigallocatechin-gallate in amyloid aggregation and neurodegenerative diseases. Front Neurosci. 2021;15:718188.
3. Yang N, Shang YX. Epigallocatechin gallate ameliorates airway inflammation by regulating Treg/Th17 imbalance in an asthmatic mouse model. Int Immunopharmacol. 2019;72:422–8.
4. March TH, Wilder JA, Esparza DC, Cossey PY, Blair LF, Herrera LK, et al. Modulators of cigarette smoke-induced pulmonary emphysema in A/J mice. Toxicol Sci. 2006;92(2):545–59.
5. Liang OD, Kleibrink BE, Schuette-Nuetgen K, Khatwa UU, Mfarrej B, Subramaniam M. Green tea epigallo-catechin-galleate ameliorates the development of obliterative airway disease. Exp Lung Res. 2011;37(7):435–44.
6. Yang N, Zhang H, Cai X, Shang Y. Epigallocatechin-3-gallate inhibits inflammation and epithelial–mesenchymal transition through the PI3K/AKT pathway via upregulation of PTEN in Asthma. Int J Mol Med. 2018;41(2):818–28.
7. Qiao J, Kong X, Kong A, Han M. Pharmacokinetics and biotransformation of tea polyphenols. Curr Drug Metab. 2014;15(1):30–6.
8. Yin C, Cheng L, Zhang X, Wu Z. Nanotechnology improves delivery efficiency and bioavailability of tea polyphenols. J Food Biochem. 2020;44(9):e13380.
9. Deng C, Zhao X, Chen Y, Ai K, Zhang Y, Gong T, et al. Engineered platelet microparticle-membrane camouflaged nanoparticles for targeting the golgi apparatus of synovial fibroblasts to attenuate rheumatoid arthritis. ACS Nano. 2022;16(11):18430–47.
10. Liu H, Su YY, Jiang XC, Gao JQ. Cell membrane-coated nanoparticles: a novel multifunctional biomimetic drug delivery system. Drug Deliv Transl Res. 2022;22:1–22.
11. Bahmani B, Gong H, Luk BT, Haushalter KJ, DeTeresa E, Previti M, et al. Intratumoral immunotherapy using platelet-cloaked nanoparticles enhances antitumor immunity in solid tumors. Nat Commun. 2021;12(1):1999.
12. Han H, Bártolo R, Li J, Shahbazi MA, Santos HA. Biomimetic platelet membrane-coated nanoparticles for targeted therapy. Eur J Pharm Biopharm. 2022;172:1–15.
13. Jin H, Li J, Zhang M, Luo R, Lu P, Zhang W, et al. Berberine-loaded biomimetic nanoparticles attenuate inflammation of experimental allergic asthma via enhancing IL-12 expression. Front Pharmacol. 2021;12:724525.
14. Albano GD, Gagliardo RP, Montalbano AM, Profita M. Overview of the mechanisms of oxidative stress: impact in inflammation of the airway diseases. Antioxid (Basel). 2022;1(11):2237.
15. Kong YR, Jong YX, Balakrishnan M, Bok ZK, Weng JKK, Tay KC, et al. Beneficial role of carica papaya extracts and phytochemicals on oxidative stress and related diseases. mini Rev Biology (Basel). 2021;10(4):287.
16. Kwak YG, Song CH, Yi HK, Hwang PH, Kim JS, Lee KS, et al. Involvement of PTEN in airway hyper-responsiveness and inflammation in bronchial asthma. J Clin Invest. 2003;111(7):1083–92.
17. Hamelmann E, Schwarze J, Takeda K, Oshiba A, Larsen GL, Irvin CG, et al. Noninvasive measurement of airway responsiveness in allergic mice using barometric plethysmography. Am J Respir Crit Care Med. 1997;156(3Pt1):766–75.
18. Bazzini C, Rossetti V, Civello DA, Sassone F, Vezzoli V, Persani L, et al. Short-and long-term effects of cigarette smoke exposure on glutathione homeostasis in human bronchial epithelial cells. Cell Physiol Biochem. 2013;32(7):129–45.
19. Liu YT, Hao HP, Xie HG, Lai L, Wang Q, Liu CX, et al. Extensive intestinal first-pass elimination and predominant hepatic distribution of berberine explain its low plasma levels in rats. Drug Metab Dispos. 2010;38(10):1779–84.
20. Naziris N, Sekowski S, Olchowik-Grabarek E, Buczkowski A, Balcerzak Ł, Chrysostomou V, et al. Biophysical interactions of mixed lipid-polymer nanoparticles incorporating curcumin: potential as antibacterial agent. Biomater Adv. 2023;144:213200.
21. Han H, Bártolo R, Li J, Ali Shahbazi M, Santos H. Biomimetic platelet membrane-coated nanoparticles for targeted therapy. Eur J Pharm Biopharm. 2022;172:1–15.
22. Ouyang S, Liu C, Xiao J, Chen X, Liu AC, Li X. Targeting IL-17A/glucocorticoid synergy to CSF3 expression in neutrophilic airway diseases. JCI Insight. 2020;5(3):e132836.
23. Ouyang S, Hsuchou H, Kastin AJ, Wang Y, Yu C, Pan W. Diet-induced obesity suppresses expression of many proteins at the blood-brain barrier. J Cereb Blood Flow Metab. 2014;34(1):43–51.
24. Jin H, Zhao Y, Yao Y, Zhao J, Luo R, Fan S, et al. Therapeutic effects of tea polyphenol-loaded nanoparticles coated with platelet membranes on LPS-induced lung injury. Biomater Sci. 2023;11(18):6223–35.
25. You H, Wei L, Sun WL, Wang L, Yang ZL, Liu Y, et al. The green tea extract epigallocatechin-3- gallate inhibits irradiation-induced pulmonary fibrosis in adult rats. Int J Mol Med. 2014;34:92–102.
26. Wang J, Fan SM, Zhang J. Epigallocatechin-3-gallate ameliorates lipopolysaccharide-induced acute lung injury by suppression of TLR4/NF-κB signaling activation. Braz J Med Biol Res. 2019;52:e8092.
27. Adcock IM, Mumby S, Glucocorticoids. Handb Exp Pharmacol. 2017;37:171–96.
28. Dos Santos AN, de Nascimento L, Gondim TR, Velo BLC, de A Rêgo MMAC, Neto RI et al. JR. Catechins as model bioactive compounds for biommedical applications. *Curr Pharm Des* 2020;26(33):4032–4047.
29. Yang CC, Yang CM. Chinese herbs and repurposing old drugs as therapeutic agents in the regulation of oxidative stress and inflammation in pulmonary diseases. J Inflamm Res. 2021;14:657–87.
30. Lakshmi SP, Reddy AT, Kodidhela LD, Varadacharyulu NC. Epigallocatechin gallate diminishes cigarette smoke-induced oxidative stress, lipid peroxidation, and inflammation in human bronchial epithelial cells. Life Sci. 2020;259:118260.
31. Ye Y, Warusawitharana H, Zhao H, Liu Z, Li B, Wu Y, et al. Tea polyphenols attenuates inflammation via reducing lipopolysaccharides level and inhibiting TLR4/NF-κB pathway in obese mice. Plant Foods Hum Nutr. 2022;77(1):105–11.
32. Almuntashiri S, Han Y, Zhu Y, Dutta S, Niazi S, Wang X, et al. Toxicity and mechanisms of Engineered nanoparticles in animals with established allergic asthma. Int J Nanomed. 2023;18:3489–508.
33. Duan H, Liu Y, Gao Z, Huang W. Recent advances in drug delivery systems for targeting cancer stem cells. Acta Pharm Sin B. 2021;11(1):55–70.
34. Mohammad-Rafiei F, Khojini JY, Ghazvinian F, Alimardan S, Norioun H, Tahershamsi Z, et al. Cell membrane biomimetic nanoparticles in drug delivery. Biotechnol Appl Biochem. 2023;70(6):1843–59.
35. Nieswandt B, Watson SP. Platelet-collagen interaction: is GPVI the central receptor? Blood. 2003;102(2):449–61.
36. Fitzgerald JR, Foster TJ, Cox D. The interaction of bacterial pathogens with platelets. Nat Rev Microbiol. 2006;4(6):445–57.
37. Wahnou H, Liagre B, Sol V, El Attar H, Attar R, Oudghiri M, Duval RE, et al. Polyphenol-based nanoparticles: a promising frontier for enhanced colorectal cancer treatment. Cancers (Basel). 2023;15(15):3826.
38. Jin H, Luo R, Li J, Zhao H, Ouyang S, Yao Y, et al. Inhaled platelet vesicle-decoyed biomimetic nanoparticles attenuate inflammatory lung injury. Front Pharmacol. 2022;13:1050224.
39. Almuntashiri S, Han Y, Zhu Y, Dutta S, Niazi S, Wang X, et al. CC16 regulates inflammation, ROS generation and apoptosis in bronchial epithelial cells during klebsiella pneumoniae infection. Int J Mol Sci. 2011;22(21):11459.
40. Plosa EJ, Benjamin JT, Sucre JM, Gulleman PM, Gleaves LA, Han W, et al. β1 integrin regulates adult lung alveolar epithelial cell inflammation. JCI Insight. 2020;5(2):e129259.
41. Kim TB, Moon KA, Lee KY, Park CS, Bae YJ, Moon HB, et al. Chlamydophila pneumoniae triggers release of CCL20 and vascular endothelial growth factor from human bronchial epithelial cells through enhanced intracellular oxidative stress and MAPK activation. J Clin Immunol. 2009;29(5):629–36.

42. Tu W, Xiao X, Lu J, Liu X, Wang E, Yuan R, et al. Vanadium exposure exacerbates allergic airway inflammation and remodeling through triggering reactive oxidative stress. Front Immunol. 2023;11:13.
43. Kaur G, Sharma A, Bhatnagar A. Role of oxidative stress in pathophysiology of rheumatoid arthritis: insights into NRF2-KEAP1 signaling. Autoimmunity. 2021;54(7):385–97.
44. Mokra D, Adamcakova J, Mokry J. Green Tea Polyphenol (-)-Epigallocatechin-3-Gallate (EGCG): a time for a New Player in the treatment of respiratory diseases? Antioxid (Basel). 2022;11(8):1566.
45. Pang X, Si J, Xu S, Li Y, Liu J. Simvastatin inhibits homocysteine-induced CRP generation via interfering with the ROS-p38/ERK1/2 signal pathway in rat vascular smooth muscle cells. Vascul Pharmacol. 2017;88:42–7.
46. Li S, Chen J, Fan Y, Wang C, Wang C, Zheng X, et al. Liposomal honokiol induces ROS-mediated apoptosis via regulation of ERK/p38-MAPK signaling and autophagic inhibition in human medulloblastoma. Signal Transduct Target Ther. 2022;7(1):49.

Publisher's Note